Obrabotka metallov (tekhnologiya, oborudovanie, instrumenty) = Metal Working and Material Science. 2024 vol. 26 no. 2 pp. 174–185
ISSN: 1994-6309 (print) / 2541-819X (online)
DOI: 10.17212/1994-6309-2024-26.2-174-185

NSTU NETI

Obrabotka metallov - Metal Working and Material Science

Journal homepage: http://journals.nstu.ru/obrabotka_metallov

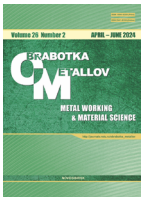

Thermal stability of extruded Mg-Y-Nd alloy structure

Anna Eroshenko[1, a,*], *Elena Legostaeva*[1, b], *Ivan Glukhov*[1, c], *Pavel Uvarkin*[1, d], *Aleksei Tolmachev*[1, e], *Yurii Sharkeev*[1, 2, f]

[1] Institute of Strength Physics and Materials Sciences SB RAS, 2/4, pr. Akademicheskii, Tomsk, 634055, Russian Federation
[2] National Research Tomsk Polytechnic University, 30 Lenin Avenue, Tomsk, 634050, Russian Federation

[a] https://orcid.org/0000-0001-8812-9287, eroshenko@ispms.ru; [b] https://orcid.org/0000-0003-3684-9930, lego@ispms.ru;
[c] https://orcid.org/0000-0001-5557-5950, gia@ispms.ru; [d] https://orcid.org/0000-0003-1169-3765, uvarkin@ispms.ru;
[e] https://orcid.org/0000-0003-4669-8478, tolmach@ispms.ru; [f] https://orcid.org/0000-0001-5037-245X, sharkeev@ispms.ru

ARTICLE INFO

Article history:
Received: 19 October 2023
Revised: 16 November 2023
Accepted: 20 March 2024
Available online: 15 June 2024

Keywords:
Mg-Y-Nd alloy
Extruded alloy
Microstructure
Phase composition
Thermal stability

Funding
The work was performed according to the Government Research Assignment for the Institute of Strength Physics and Materials Science of the Siberian Branch of the Russian Academy of Sciences (ISPMS SB RAS), project No. FWRW-2021-0004. Experimental research was conducted using the equipment of the Common Use Center "Nanotech" at the Institute of Strength, Physics, and Materials Science, SB RAS (ISPMS SB RAS, Tomsk, Russia).

Acknowledgements
The authors are grateful to engineer *Juergen Schmid* (Department of Electrochemistry, Innovent Technology Development, Germany) and researcher. *Chebodeva V.V.* (IPPM SB RAS) for assistance in carrying out a number of experimental works.

ABSTRACT

Introduction. Today, bioresorbable magnesium alloys possessing the required physical, mechanical, corrosion, and biological properties, are promising materials for orthopedic and cardiovascular surgery. The addition of rare earth elements such as yttrium, neodymium, and cerium to magnesium alloys improves its properties. Compared to widely used titanium alloys, magnesium alloys have a number of advantages. Bioresorbable materials slowly dissolve in the body, and recurrent operation to remove the implant is not needed. Biocompatible magnesium alloys have a fairly low elastic modulus (10 to 40 GPa), approaching to that of cortical bone, that reduces the contact stress in the bone-implant system. At the same time, strength properties of magnesium alloys alloyed with rare earth elements do not always meet the requirements for medical applications. Severe plastic deformation, for example, equal channel angular pressing, torsion under quasi-hydrostatic pressure, uniaxial forging, extrusion, is therefore very promising technique to gain the high level of mechanical properties of metals and alloys. Severe plastic deformation of magnesium alloys improves its structural strength by 2.5 times due to the generation of an ultrafine-grained and/or fine-grained structure. The issues related to the study of heat resistance, structure and phase composition of magnesium alloys with appropriate strength are relevant. **Purpose of the work** is to determine the influence of thermal effects on the microstructure of the extruded *Mg-Y-Nd* alloy. **Methodology.** The extruded *Mg-2.9Y-1.3Nd* alloy (95.0 wt. % *Mg*, 2.9 wt. % *Y*, 1.3 wt. % *Nd*, ≤ 0.2 wt. % *Fe*, ≤ 0 wt. % *Al*) is investigated in this paper. The thermal stability of the alloy microstructure is studied after annealing at 100, 300, 350, 450 and 525 °C in argon for one hour. The microstructure and phase composition are investigated using optical, transmission and scanning electron microscopes and analyzed on an X-ray diffractometer. **Results and discussion.** The extruded *Mg-2.9Y-1.3Nd* alloy has the bimodal fine-grained microstructure. It is found that along with the stable α-*Mg* phase, the alloy structure consists of $Mg_{24}Y_5$ intermetallic particles and β-, β′-, and β1-phase precipitates. Annealing in the temperature range of 100–450 °C for one hour has no effect on the structure of the *Mg-2.9Y-1.3Nd* alloy, but promotes the growth in the linear dimensions of β-, β′-, and β1-phases precipitates. In the temperature range of 300–450 °C, the morphology of β-, β′,- and β1-phases changes, while the average grain size of the major α-phase remains unchanged. Annealing at 525 °C leads to a notable transformation of the bimodal microstructure of the alloy, which is associated with the intensive growth in the grain size of the α-phase, $Mg_{24}Y_5$ particles, and β-, β′-, and β1-phases precipitates. Annealing in the temperature range of 100–450 °C leads to an increase in the linear dimensions of $Mg_{24}Y_5$ particles, β-, β′-, and β1-phases precipitates and bimodal microstructure of the *Mg-2.9Y-1.3Nd* alloy remains unchanged.

For citation: Eroshenko A.Yu., Legostaeva E.V., Glukhov I.A., Uvarkin P.V., Tolmachev A.I., Sharkeev Yu.P. Thermal stability of extruded Mg-Y-Nd alloy structure. *Obrabotka metallov (tekhnologiya, oborudovanie, instrumenty) = Metal Working and Material Science*, 2024, vol. 26, no. 2, pp. 174–185. DOI: 10.17212/1994-6309-2024-26.2-174-185. (In Russian).

*** Corresponding author**
Eroshenko Anna Yu., Ph.D. (Engineering), Senior research fellow
Institute of Strength Physics and Materials Sciences SB RAS,
2/4, pr. Akademicheskii,
634055, Tomsk, Russian Federation
Tel.: +7 3822 28-69-11, **e-mail:** eroshenko@ispms.ru

Introduction

Today, bioresorbable magnesium alloys, possessing the required physical, mechanical, corrosion, and biological properties, are promising materials for orthopedic and cardiovascular surgery [1–8]. The addition of rare earth elements (*REE*) such as yttrium, neodymium, and cerium to magnesium alloys, improves its properties [9]. Yttrium provides the formation of stable phases with magnesium, thereby improving the alloy strength and plasticity. Neodymium and cerium improve the corrosion resistance and thermal stability of these alloys.

Compared to widely used titanium alloys, magnesium alloys have a number of advantages. Firstly, bioresorbable materials slowly dissolve in the body, and recurrent operation to remove the implant is not needed [2–4]. Secondly, biocompatible magnesium alloys do not cause such negative reactions in the body as inflammatory processes, implant failure, and others. Thirdly, its elastic modulus is rather low (10–40 GPa), approaching to that of cortical bone, that reduces the contact stress in the bone-implant system [3, 4]. In this respect, severe plastic deformation, for example, equal channel angular pressing, torsion under quasi-hydrostatic pressure, uniaxial forging (*abc*-pressing), extrusion, is therefore a very promising technique to gain the high level of mechanical properties of metals and alloys [10–16]. Severe plastic deformation of magnesium alloys improves its structural strength by 2.5 times due to the generation of an ultrafine-grained and/or fine-grained structure.

Mg-Y-Nd-based (commercial *WE43*, *WE54*) deformable alloys with the addition of yttrium and neodymium, are used in the production of units and parts for aircraft control systems [16]. Rare earth-based (neodymium, yttrium, cadmium, lanthanum) magnesium alloys are mostly used in aircraft and space equipment, since its refractoriness ranges from 250 to 300 °C [17–19].

Relevant are issues relating to the exploration of thermal stability, structure and phase composition of magnesium alloys with the appropriate strength properties. This is determined by the structural variety of magnesium alloys, both in cast and deformed states, which significantly affects its physical and mechanical properties. It is thus important to create high-strength magnesium alloys and analyze its thermal stability, structure, and phase composition.

The aim of this work is to determine the thermal effect on the microstructure and phase composition of the extruded *Mg-Y-Nd* system alloy.

Materials and research methodology

The *Mg-2.9Y-1.3Nd* alloy (95.0 wt.% *Mg*, 2.9 wt.% *Y*, 1.3 wt.% *Nd*, ≤0.2 wt.% *Fe*, ≤0 wt.% *Al*) (commercial *WE43* alloy) was used in experiments. The alloy was obtained by permanent mold casting [20]. The alloy specimens were subjected to severe plastic deformation (extrusion at 350 °C) for the grain refinement and enhancement of mechanical properties. The diameter of the initial bars was 60 mm, and after extrusion it decreased to 14 mm. True strain was determined by logarithm of the ratio of the initial and final thickness of the specimens. Accumulated logarithmic strain after specimen treatment was 1.46.

The microstructure and phase composition of alloy specimens were studied on an *Axio Observer Inverted Microscope* (*Carl Zeiss*, Germany), a *JEM-2100* (*JEOL Ltd.*, Japan) high-resolution transmission electron microscope (*TEM*) combined with X-ray microanalysis, and *Zeiss EVO 50* (Germany) scanning electron microscope (*SEM*). The X-ray phase (*XRD*) analysis was carried out using *DRON-7* diffractometer (*Burevestnik*, Russia). Measurements were conducted using copper radiation (K_α). Medium sizes of grains, subgrains, fragments were detected on micrographs using the secant method [21].

The thermal stability of the alloy microstructure was studied after annealing at 100, 300, 350, 450, 525 °C in argon for one hour. According to [20–24], the thermal treatment of *Mg-Y-Nd* system alloys at 100 to 525 °C provides the formation of various structural and phase transformations and a complex behavior of the temperature dependence of the heat capacity.

Results and discussion

Figure 1 presents optical and *TEM* images of bimodal microstructure of the extruded *Mg-2.9Nd-1.3Y* alloy, which can be clearly observed in Fig. 1, *a*. *TEM* observations show that the microstructure of the extruded *Mg-Nd-Y* alloy is based on the hexagonal close packed (*HCP*) α-*Mg* phase solid solution (see Fig. 1, *b*) and intermetallic compounds based on *Mg*, *Nd*, *Y*. Intermetallic compounds can be observed inside grains and along grain boundaries (Fig. 1, *b, c, d, e, f, g*). According to [25–30], in *Mg-Y-Nd* system alloys these phases are identified as body centered cubic $Mg_{24}Y_5$ particles and three types of metastable phases. These phases include a face centered cubic (*FCC*) eutectic equilibrium β-phase ($Mg_{14}Nd_2Y$) in the form of a network, an orthorhombic β′-phase ($Mg_{12}YNd$) with a globular morphology, and a *FCC* β1-phase (Mg_3NdY) lamellas. Note that metastable β or β1 phases are considered to be the main reinforcing agents, which are usually present in the annealed *WE43* alloy [25–29]. According to [28], in the deformed magnesium alloy *WE43* during a long-term aging the metastable β1-phase is transformed into the equilibrium β-phase.

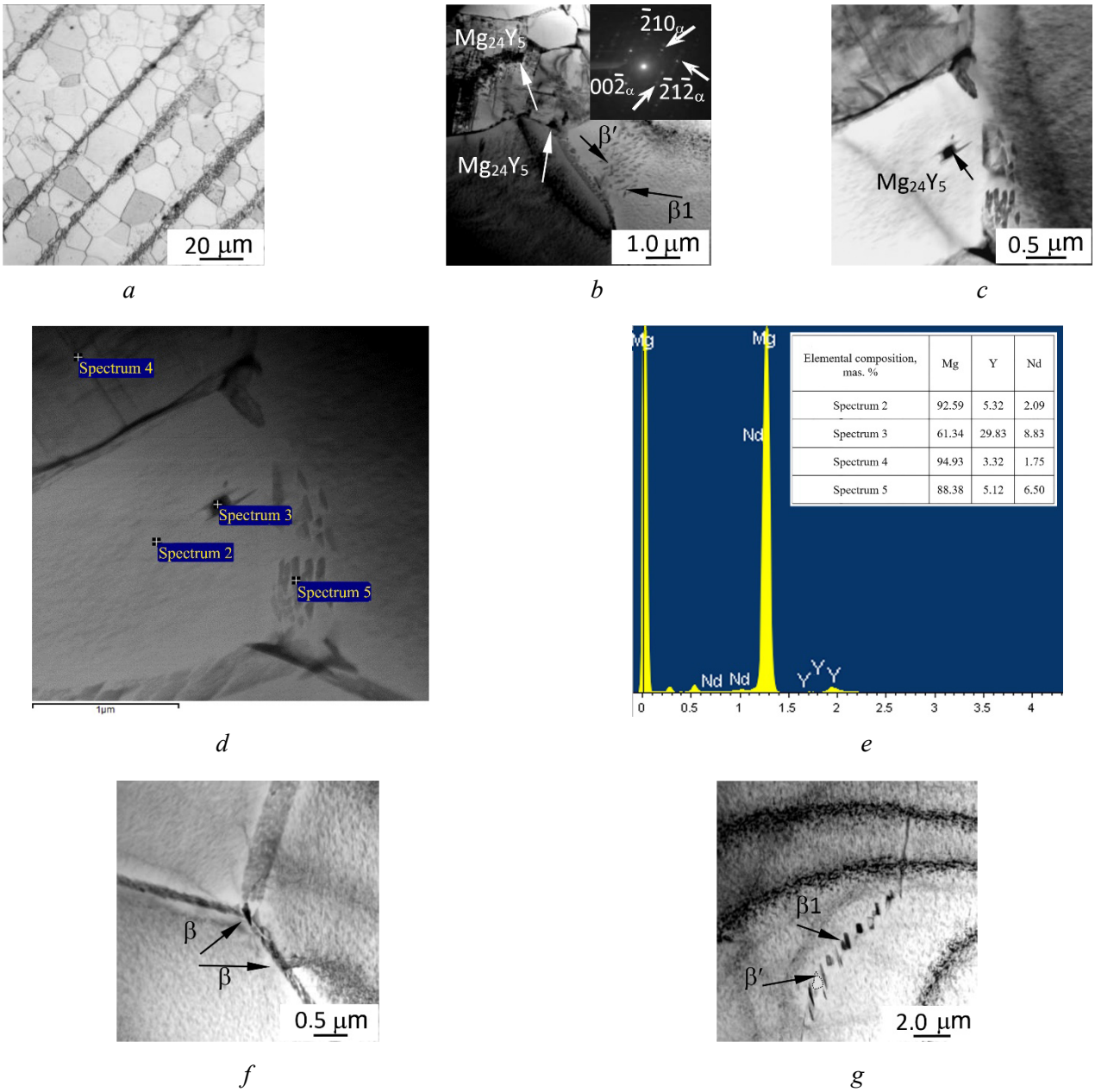

Elemental composition, mas. %	Mg	Y	Nd
Spectrum 2	92.59	5.32	2.09
Spectrum 3	61.34	29.83	8.83
Spectrum 4	94.93	3.32	1.75
Spectrum 5	88.38	5.12	6.50

a *b* *c*

d *e*

f *g*

Fig. 1. Optical (*a*) and bright field TEM images (*b, c, d, f, g*), energy dispersive spectrums and elemental composition (*d, e*) of extruded Mg-2.9Y-1.3Nd alloy. Insert: selected area diffraction pattern

The optical image shows two types of structural elements, namely coarse (~17 μm) and ultra-fine (~1 μm) grains, the latter represent textured bands. The volume fraction of ultra-fine grains is 50 % of the total volume.

Intermetallic particles are additionally deduced from the energy-dispersive X-ray (*EDX*) analysis of the elemental composition shown in Fig. 1, *c*, *d*. *EDX* spectra in this figure are obtained at different points of thin specimen. $Mg_{24}Y_5$ particles are high in yttrium (30 wt.%) and locate mostly inside grains (Fig. 1, *e*). In the extruded alloy, $Mg_{24}Y_5$ particles are mostly irregular polyhedrons with the average size of 0.6 μm. According to *TEM* images, the volume fraction of these particles is not over 2 %. The eutectic equilibrium β-phase is localized along the grain boundaries as a network of precipitates up to 0.3–0.4 μm thick. This phase is also irregular polyhedrons and, to a lesser extent, regular tetrahedrons presented in Fig. 1, *f*. The medium size of β′-phase globules is 0.2 μm. The length and width of the β1-phase vary within the range of 0.06–0.30 μm and 0.03–0.04 μm, respectively (Fig. 1, *g*). Note that β1-phase lamellas are positioned in the same direction. In the β-phase, yttrium and neodymium amount to (3.54–7.18) wt. % and (2.26–9.59) wt. %, respectively. In the β′-phase, the content ranges between 3.21 and 5.39 wt. % for yttrium and between 1.83 and 2.07 wt. % for neodymium. In β1-phases, yttrium and neodymium range between (3.32–5.27) wt. % and (1.75–8.46) wt. %, respectively. The β′-phase contributes to the greatest extent to the increase in the mechanical properties of *Mg-Y-1Nd* alloys due to its strain hardening [24].

Figure 2 presents optical images of the *Mg-2.9Nd-1.3Y* alloy microstructure after annealing in the temperature range of 100–450 °C. As can be seen in this figure, the bimodal microstructure does not change after annealing (Fig. 2, *a-d*). Finer grains of the α-phase range in size from 0.2 to 5.0 μm. After annealing, its medium size does not change and is equal to 1 μm.

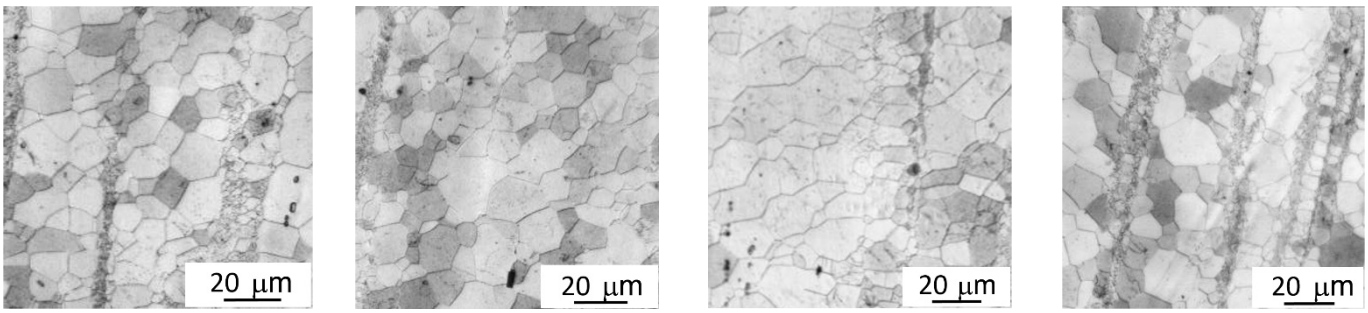

a *b* *c* *d*

Fig. 2. Optical images of extruded *Mg-2.9Y-1.3Nd* alloy microstructure after annealing at different temperatures: *a* – 100 °C; *b* – 300 °C; *c* – 350 °C; *d* – 450 °C

Note that the formation of the fine-grained structure in the extruded *Mg-2.9Y-1.3Nd* alloy significantly improves its yield strength and tensile strength up to 150 and 230 MPa, respectively. For the recrystallized structure obtained after 525 °C annealing for 6 hours, these parameters are 220 and 340 MPa, respectively [22]. The alloy plasticity also increases from 12 to 21 %.

Figure 3 contains *TEM* images of the alloy microstructure after annealing at different temperatures. On bright field images, one can see four types of intermetallic inclusions after 100 °C annealing, namely $Mg_{24}Y_5$ particles (Fig. 3, *a*) and β-, β′- and β1-phases (Fig. 3, *b*), as in the extruded structure. Unlike the extruded structure, the medium size of $Mg_{24}Y_5$ particles grows up to 0.9 μm, and there is a slight increase in the width of the subgrain β-phase boundary, which varies in the range (0.4–0.5) μm (Fig. 3, *a, b*). Linear dimensions of secondary β′- and β1-phase precipitates do not change.

The temperature growth up to 300 °C leads to a further increase in the medium size of $Mg_{24}Y_5$ particles from 0.9 to 1.2 μm and morphology transformation of some particles from irregular polyhedrons to regular tetrahedrons, as presented in Fig. 3, *c*. This indicates the occurrence of recrystallization process. The microstructure in Fig. 3, *d–f*, includes all types of secondary non-equilibrium phases described above. The network width of the grain boundary increases up to 1.2–1.7 μm and consists of the eutectic β-phase (Fig. 3, *d*). In Fig. 3, *e*, *f*, one can see β′-phase globules and β1-phase lamellas. A significant growth in β1-

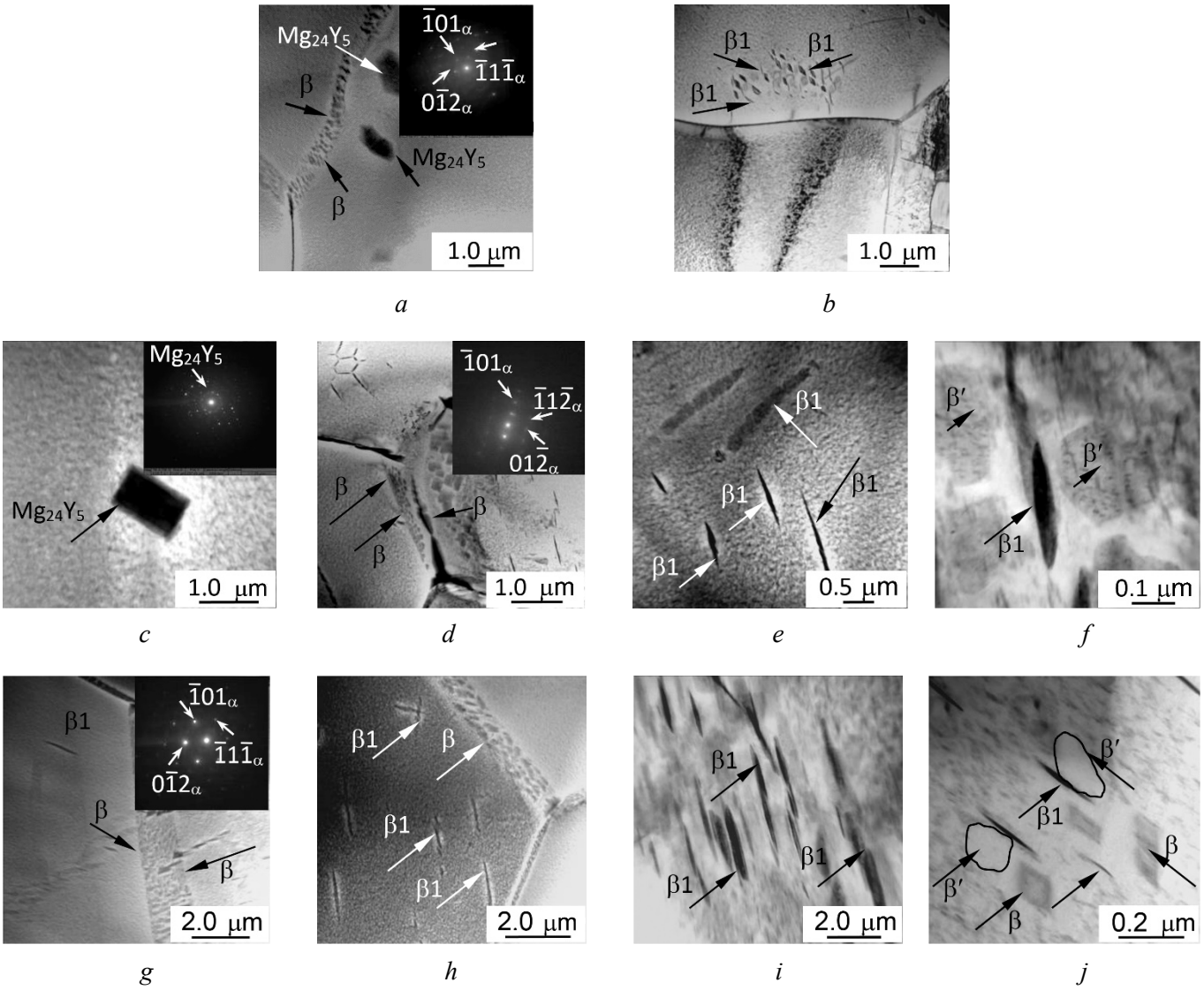

Fig. 3. Bright field *TEM* images with corresponding microdiffraction patterns of extruded *Mg-2.9Nd-1.3Y* alloy microstructure after annealing at:

a, b – 100 °C; *c–f* – 300 °C; *g, h* – 350 °C; *i, j* – 450 °C

phase lamellas is observed with coarsening $Mg_{24}Y_5$ particles, i.e., the length grows from 0.3 to 0.8 μm and the width expands from 0.04 to 0.07 μm (Fig. 3, *e*).

The average cross-sectional dimension of β′-phase precipitates is 0.2 μm (Fig. 3, *f*). It is notable that the length and width of smaller β1-phase lamellas localizing nearby the grain boundaries, vary from 0.3 to 0.8 μm and from 0.02 to 0.08 μm, respectively. It is worth noting that according to [24], the formation of β1-phase lamellas is determined by the presence of β′-phase globules.

TEM observations [23] revealed β′-, and β1-phases precipitates in the *Mg-Y-Nd* system alloy after annealing at 250 °C. The latter led to the formation of metastable β′-, and β1-phases followed by the formation of the equilibrium β-phase. It is shown that the β1-phase represented β′-phase nuclei and could generate much shear energy and shear energy accommodation. During a long-term annealing, e.g., aging at 250 °C, the β1-phase transferred to the equilibrium β-phase.

Annealing at 350 °C provides the width expansion of continuous subgrain boundary in the range of 0.8 to 1.7 μm (Fig. 3, *g*). The average length and width of β1-phase lamellas are respectively 0.6 and 0.03 μm. The average size of β′-phase precipitates is 0.2 μm, as it is demonstrated in Fig. 3, *h*. Annealing at 350 °C promotes aggregation of $Mg_{24}Y_5$ intermetallic particles.

Annealing at 450 °C results in widening of the eutectic β-phase network up to 2 μm. In this case, most of $Mg_{24}Y_5$ particles are tetrahedrons having the medium size of 1.3 μm. Localized regions consist of typi-

cal β′-phase globules and β1-phase lamellas. The average size of β′-phase precipitates is 0.2 μm, while the length and width of the β1-phase lamellas vary from 0.6 to 0.7 and from 0.02 to 0.05 μm, respectively (Fig. 3, *i*). Eutectic β-phase particles are well-defined rhombs, as it is shown in Fig. 3, *j*. Annealing at 450 °C provides further coarsening of $Mg_{24}Y_5$ intermetallic particles. At higher annealing temperatures, β′-, and β1-phases particles become larger or are replaced by the stable β-phase according to β′ → β or β1→ β phase transformations [24, 27–30].

After annealing at 525 °C, the alloy microstructure undergoes transformation. According to optical and *SEM* microscopy the structure becomes more homogeneous (Fig. 4, *a*, *b*).

The average size of the base α-phase reaches 32 μm. There are no textured bands consisting of magnesium fine grains, which indicates intensive recrystallization processes. Bright field *TEM* images demonstrate four types of intermetallic inclusions, namely $Mg_{24}Y_5$ particles (Fig. 4, *c*) and β-, β′-, and β1-phases (Fig. 4, *d*, *e*) similar to those observed after annealing at 450 °C. The medium size of $Mg_{24}Y_5$ particles is 1.4 μm, and its shape is a regular tetrahedron. The width of the subgrain β-phase boundary expands and ranges between 0.6 and 1.2 μm. The length and width of β1-phase lamellas vary from 1.1 to 6.2 and from 0.4 to 1 μm, respectively. The average size of β′-phase precipitates is 0.3 μm.

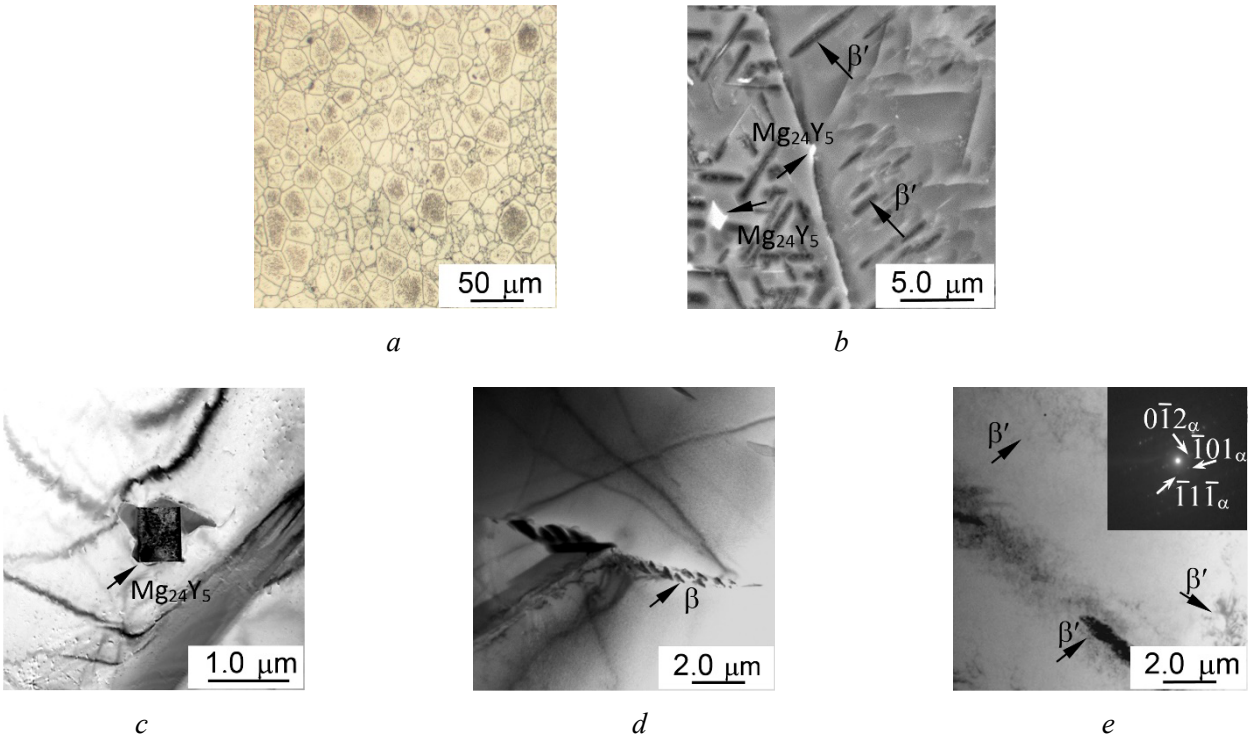

a *b* *c* *d* *e*

Fig. 4. Optical, *SEM* and *TEM* images of *Mg-2.9Y-1.3Nd* alloy microstructure after annealing at 525°C:
a, b – optical and *SEM* images; *c–e* – bright field *TEM* images with corresponding microdiffraction pattern

The dependence of the average size of structural elements of various phases on the annealing temperature is shown in Fig. 5. When annealing in the temperature range 100–450 °C, the average grain size of the α-phase does not change, but at the same time there is a slight increase in the particle size of $Mg_{24}Y_5$ particles and precipitates of β-, β′-, and β1-phases, which indicates its thermal instability at the above temperatures. At a temperature of 525 °C, there is a noticeable increase in both the grain size of the matrix α-phase of magnesium, and $Mg_{24}Y_5$ particles, and precipitates of β-, β′-, and β1-phases. Note that the $Mg_{24}Y_5$ particles and precipitates of β-,β′-, and β1-phases are present at fairly high temperatures, up to 525 °C. It should be noted that $Mg_{24}Y_5$ particles and β-, β′-, and β1-phases in the *Mg-Nd-Y* system alloy, are thermally stable at rather high annealing temperatures reaching 525 °C.

In Fig. 6, one can see fragments of *XRD* patterns of the extruded *Mg-2.9Y-1.3Nd* alloy and annealed at temperatures of 100–525 °C.

According to *XRD* patterns of the extruded *Mg-2.9Y-1.3Nd* alloy, high intensity peaks belong to the *HCP* α-*Mg* phase solid solution. After annealing at 100–450 °C, *XRD* patterns do not change, whereas at a temperature of 525 °C, the X-ray line width of the α-phase notably decreases and the intensity redistribution occurs in (100), (101) and (101) directions, indicating to intensive recrystallization processes accompanied by the grain growth. In addition to the major α-*Mg* phase, *TEM* investigations show the presence of fine-grained $Mg_{24}Y_5$ intermetallic particles and β-, β′-, and β1-phases precipitates in the alloy, which cannot be identified by the X-ray spectroscopy.

Thus, we can conclude, that the bimodal microstructure of the *Mg-2.9Y-1.3Nd* alloy does not change after one hour annealing in the temperature range of 100–450 °C, although a slight growth is observed for fine-grained $Mg_{24}Y_5$ particles and β-, β′-, and β1-phases precipitates with its morphology transformation.

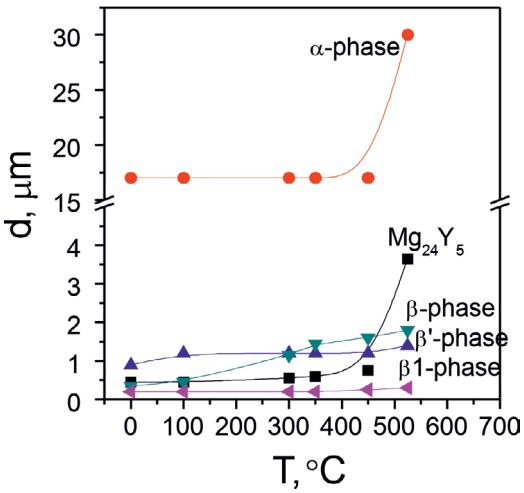

Fig. 5. The dependences of the average size of structural elements of phases on the annealing temperature

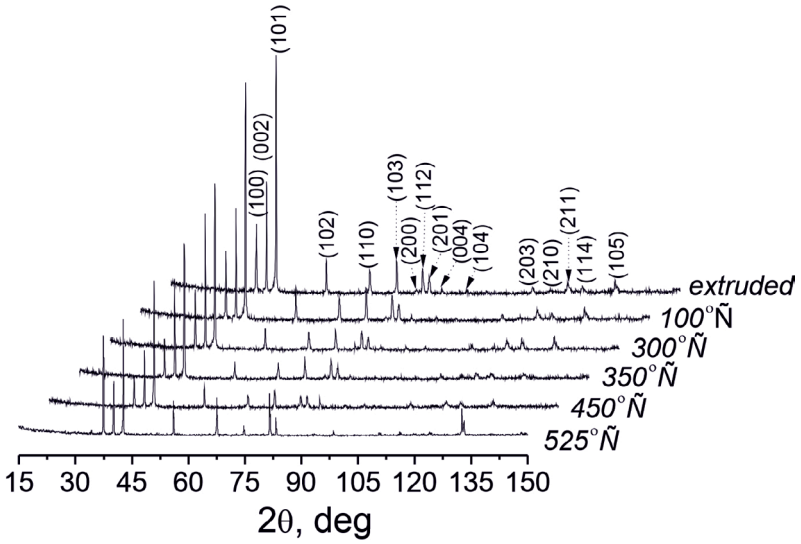

Fig. 6. Fragments of *XRD* patterns of extruded *Mg-2.9Y-1.3Nd* alloy and after annealing

Conclusions

In conclusion, this study has shown the formation of the bimodal microstructure in the extruded *Mg-2.9Y-1.3Nd* alloy. The microstructure consisted of a α-phase and textured bands with an average grain size of 17 μm and 1 μm, respectively. It was found that along with the major stable α-Mg phase, the alloy microstructure comprised $Mg_{24}Y_5$ intermetallic particles and precipitates of the of three types phases. Annealing within 100–450 °C for 1 hour had no effect on the general structure of the *Mg-2.9Y-1.3Nd* alloy, but promoted the growth in the linear dimensions of precipitates of β-, β′-, and β1-phases. It is shown that within 300–450 °C, the morphology of β-, β′-, and β1-phases changed while maintaining the average size of the α-phase. Annealing at 525 °C resulted in a significant transformation of the bimodal microstructure, conditioned by the recrystallization process and intensive grain growth of the major phase, $Mg_{24}Y_5$ intermetallic particles, and secondary precipitates of β-, β′-, and β1-phases.

References

1. Niinomi M., Liu Y., Nakai M., Lui H., Li H. Biomedical titanium alloys with Young's moduli close to that of cortical bone. *Regenerative Biomaterials*, 2016, vol. 3, pp. 173–185. DOI: 10.1093/rb/rbw016.

2. Uppal G., Thakur A., Chauhan A., Bala S. Magnesium based implants for functional bone tissue regeneration – A review. *Journal of Magnesium and Alloys*, 2022, vol. 10 (2), pp. 356–386. DOI: 10.1016/j.jma.2021.08.017.

3. Zhao D., Witte F., Lu F., Wang J., Li J., Qin L. Current status on clinical applications of magnesium-based orthopaedic implants: A review from clinical translational perspective. *Biomaterials*, 2016, vol. 112, pp. 287–302. DOI: 10.1016/j.biomaterials.2016.10.017.

4. Plaass C., Von Falck C., Ettinger S., Sonnow L., Calderone F., Weizbauer A., Reifenrath J., Claassen L., Waizy H., Daniilidis K., Stukenborg-Colsman C., Windhagen H. Bioabsorbable magnesium versus standard titanium compression screws for fixation of distal metatarsal osteotomies – 3 year results of a randomized clinical trial. *Journal of Orthopaedic Science*, 2018, vol. 23 (2), pp. 321–327. DOI: 10.1016/j.jos.2017.11.005.

5. Walker J., Shadanbaz S., Woodfield T., Staiger M., Dias G. Magnesium biomaterials for orthopedic application: A review from a biological perspective. *Journal of Biomedical Materials Research. Part B: Applied Biomaterials*, 2014, vol. 102 (6), pp. 1316–1331. DOI: 10.1002/jbm.b.33113.

6. Witte F., Hort N., Vogt C., Cohen S., Kainer K., Willumeit R., Feyerabend F. Degradable biomaterials based on magnesium corrosion. *Current Opinion in Solid State and Materials Science*, 2008, vol. 12 (5–6), pp. 63–72. DOI: 10.1016/j.cossms.2009.04.001.

7. Zheng Y., Gu X., Witte F. Biodegradable metals. *Materials Science and Engineering: Reports*, 2014, vol. 77, pp. 1–34. DOI: 10.1016/j.mser.2014.01.001.

8. Sun H.F., Li C.J., Fang W.B. Evolution of microstructure and mechanical properties of Mg–3.0Zn–0.2Ca–0.5Y alloy by extrusion at various temperatures. *Journal of Materials Processing Technology*, 2016, vol. 229, pp. 633–640. DOI: 10.1016/j.jmatprotec.2015.10.021.

9. Wang J., Dou J., Wang Z., Hu C., Yu H., Chen C. Research progress of biodegradable magnesium-based biomedical materials: A review. *Journal of Alloys and Compounds*, 2022, vol. 923, p. 66377. DOI: 10.1016/j.jallcom.2022.166377.

10. Yurchenko N.Yu., Stepanov N.D., Salishchev G.A., Rokhlin L.L., Dobatkin S.V. Effect of multiaxial forging on microstructure and mechanical properties of Mg-0.8Ca alloy. *IOP Conference Series: Materials Science and Engineering*, 2014, vol. 63, pp. 1–7. DOI: 10.1088/1757-899X/63/1/012075.

11. Merson D.L., Brilevsky A.I., Myagkikh P.N., Markushev M.V., Vinogradov A. Effect of deformation processing of the dilute Mg-1Zn-0.2Ca alloy on the mechanical properties and corrosion rate in a simulated body fluid. *Letters on Materials*, 2020, vol. 10 (2), pp. 217–222. DOI: 10.22226/2410-3535-2020-2-217-222.

12. Zeng Z., Nie J., Xu S., Davies C., Birbilis N. Super-formable pure magnesium at room temperature. *Nature Communications*, 2017, vol. 8, p. 972. DOI: 10.1038/s41467-017-01330-9.

13. Bohlen J., Yi S., Letzig D., Kainer K. Effect of rare earth elements on the microstructure and texture development in magnesium-manganese alloys during extrusion. *Materials Science and Engineering: A*, 2010, vol. 527, pp. 7092–7098. DOI: 10.1016/j.msea.2010.07.081.

14. Atwell L., Barnett R. Extrusion limits of magnesium alloys. *Metallurgical and Materials Transactions A*, 2007, vol. 38, pp. 3032–3041. DOI: 10.1007/s11661-007-9323-2.

15. Kulyasova O., Islamgaliev R., Mingler B., Zehetbauer M. Microstructure and fatigue properties of the ultrafine-grained AM60 magnesium alloy processed by equal-channel angular pressing. *Materials Science and Engineering A*, 2009, vol. 503 (1–2), pp. 176–180. DOI: 10.1016/j.msea.2008.03.057.

16. Ben-Hamu G., Eliezer D., Wagner L. The relation between severe plastic deformation microstructure and corrosion behavior of AZ31 magnesium alloy. *Journal of Alloys and Compounds*, 2009, vol. 468, pp. 222–229. DOI: 10.1016/j.jallcom.2008.01.084.

17. Kablov E.N. Innovation developments of VIAM on organization of 'Strategic directions of the development of materials and technologies of their processing for the period to 2030 year. *Aviation Materials and Technologies*, 2015, vol. 1 (34), pp. 3–33. DOI: 10.18577/2071–9140-2015-0-1-3-33.

18. Rokhlin L.L. *Magnesium alloys containing rare earth metals: structure and properties*. London, Taylor and Francis Inc., 2003. 245 p. ISBN 9780429179228.

19. Bai J., Yang Y., Wen C., Chen J., Zhou G., Jiang B., Peng X., Pan F. Applications of magnesium alloys for aerospace: A review. *Journal of Magnesium and Alloys*, 2023, vol. 11 (10), pp. 3609–3619. DOI: 10.1016/j.jma.2023.09.015.

20. Wang W., He L., Yang X., Wang D. Microstructure and microhardness mechanism of selective laser melting Mg-Y-Sm-Zn-Zr alloy. *Journal of Alloys and Compounds*, 2021, vol. 868, p. 159107. DOI: 10.1016/j.jallcom.2021.159107.

21. ASTM E1382-97. *Standard test methods for determining average grain size using semiautomatic and automatic image analysis.* West Conshohocken, PA, ASTM International, 2016. 24 p.

22. Legostaeva E., Eroshenko A., Vavilov V., Skripnyak V.A., Luginin N., Chulkov A., Kozulin A., Skripnyak V.V., Schmidt J., Tolmachev A., Uvarkin P., Sharkeev Y. Influence of severe plastic deformation by extrusion on microstructure, deformation and thermal behavior under tension of magnesium alloy Mg-2.9Y-1.3Nd. *Metals*, 2023, vol. 13, p. 988. DOI: 10.3390/met13050988.

23. Nie J., Muddle B. Characterization of strengthening precipitate phases in a Mg–Y–Nd alloy. *Acta Materialia*, 2000, vol. 48 (8), pp. 1691–1703. DOI: 10.1016/S1359-6454(00)00013-6.

24. Calado L.M., Carmezim M.J., Montemor M.F. Rare earth based magnesium alloys – A review on WE series. *Frontiers in Materials*, 2022, vol. 8, p. 808906. DOI: 10.3389/fmats.2021.804906.

25. Hort N., Salgado-Ordoric M.A., Kainer K. Magnesium permanent mold castings optimization. *Materials Science Forum*, 2011, vol. 690, pp. 65–68. DOI: 10.4028/www.scientific.net/MSF.690.65.

26. Nie J.-F. Precipitation and hardening in magnesium alloys. *Metallurgical and Materials Transactions A*, 2012, vol. 43, pp. 3891–3939. DOI: 10.1007/s11661-012-1217-2.

27. Mengucci P., Barucca G., Riontino G., Lussana D., Massazza M., Ferragut R., Hassan Aly E. Structure evolution of a WE43 Mg alloy submitted to different thermal treatments. *Materials Science and Engineering: A*, 2008, vol. 47, pp. 37–44. DOI: 10.1016/j.msea.2007.06.016.

28. Kang Y., Huang Z., Wang S., Yan H., Chen R., Huang J. Effect of pre-deformation on microstructure and mechanical properties of WE43 magnesium alloy II: Aging at 250 and 300 °C. *Journal of Magnesium and Alloys*, 2020, vol. 8, pp. 103–110. DOI: 10.1016/j.jma.2019.11.012.

29. Kubásek J., Dvorský D., Čavojský M., Roudnická M., Vojtech D. WE43 magnesium alloy – material for challenging applications. *Kovove Materialy = Metallic Materials*, 2019, vol. 57 (3), pp. 159–165. DOI: 10.4149/km_2019_3_159.

30. Ladd M., Palmer R. *Structure determination by X-ray crystallography: Analysis by X-rays and neutrons*. New York, Springer, 2013. 784 p. ISBN 1461439566.

Conflicts of Interest

The authors declare no conflict of interest.